15th World Congress on Computational Mechanics (WCCM-XV)
8th Asian Pacific Congress on Computational Mechanics (APCOM-VIII)
Virtual Congress: 31 July – 5 August 2022
S. Koshizuka (Ed.)

NEW CALCULATION SCHEME

FOR COMPRESSIBLE EULER EQUATION

TAKASHI NAKAZAWA

[1]Osaka University
Machikaneyama-cho, Toyonaka, Osaka, Japan
nakazawa@sigmath.es.osaka-u.ac.jp

Key words: Finite element method, Galaekin method, Compressible Euler equation, AMR

Abstract. *In this paper, numerical demonstrations of a modified compressible Euler system are shown, where the bubble function element stabilization method together with adaptive mesh refinement is introduced for increasing numerical stability and numerical accuracy. For a test case, NACA0012 is selected as a domain of interest, and numerical results using finite elements of P1-P1b-P1 and P2-P2b-P2 for density-velocity-pressure were compared at AOA=1.25 and Mach number 0.8. As a result, the shock wave is not found on the upper-end and the lower-end of NACA0012 in the former, and on the other hand the latter is adequate numerical result and relative errors of Cl, Cd with previous study are 1.197% and 0.15376%. The mathematical model is much simpler than the compressible Euler equation, because they are advection equations for a density, a velocity, and a pressure with each external forces. Therefore, the material derivative is considered for time stepping, and the characteristic curve method can be used for decreasing calculation cost.*

1 INTRODUCTION

In this work, we address the numerical solution of the compressible Euler equation.

$$\frac{\partial \rho}{\partial t} + \nabla \cdot (\rho \boldsymbol{u}) = 0, \tag{1}$$

$$\frac{\partial \rho \boldsymbol{u}}{\partial t} + \nabla \cdot (\rho \boldsymbol{u} \otimes \boldsymbol{u}) + \nabla p = 0, \tag{2}$$

$$\frac{\partial \rho E}{\partial t} + \nabla \cdot (\rho E \boldsymbol{u}) + \nabla \cdot (p \boldsymbol{u}) = 0, \tag{3}$$

$$\rho \geq 0, e \geq 0, p = P(\rho, e), E = \frac{1}{2}|\boldsymbol{u}|^2, \tag{4}$$

where $\boldsymbol{u} = \left[u_x, u_y\right]^{\mathrm{T}}, \rho, p, E$ and e denote the velocity, the density, the pressure, the total

energy, and the internal energy, respectively. The function $\mathrm{P}(\rho, e)$ is the equation of the state for an ideal gas, which we extend by zero for negative ρ and e, for the sole purpose of the mathematical study of the scheme:

$$\mathrm{P}(\rho, e) = \begin{cases} (\gamma - 1)\rho e & \text{if } \rho \geq 0, e \geq 0, \\ 0 & \text{otherwise,} \end{cases} \tag{5}$$

where γ is the ratio of the specific heats of the gas. The problem is defined over $\Omega \times (0, T)$. The system is complemented by initial conditions for ρ, e and $\boldsymbol{u}$, which are denoted by ρ_0, e_0 and $\boldsymbol{u}_0$ with $\rho_0 > 0$ and $e_0 > 0$. In the study of the numerical scheme, we shall consider for simplicity the boundary condition $\boldsymbol{u} \cdot \boldsymbol{n} = 0$, where $\boldsymbol{n}$ stands for the outward normal vector to the boundary, but other conditions are also easily implemented. One of the models used for the numerical simulation of a compressible flow is based on the assumption that the flow is inviscid and adiabatic. This means that in gas we neglect the inertial friction and heat transfer. Inviscid adiabatic flow is described by the continuity equation. the Euler equation of motion and the energy equation, to which we add closing thermodynamical relations. This complete system is usually called the Euler equations in Eqs. (1-4). Variables and parameters used in this paper are listed in Table 1.

Table 1: Variables and parameters.

Symbol	Parameters	Values
γ	The ratio of the specific heats of the air	1.4
R	Gas constant	$259.825\ (\mathrm{m}^2/\mathrm{s}^2\mathrm{K})$
p_∞	Pressure at free stream condition	$26400\ (\mathrm{Kg}/\mathrm{s}^2)$
ρ_∞	Density at free stream condition	$0.41\ (\mathrm{Kg}/\mathrm{m}^3)$
T_∞	Temperature at free stream condition	$\frac{p_\infty}{\rho_\infty R} \approx 247.821(K)$
U_∞	Velocity at free stream	$\sqrt{\frac{\gamma p_\infty}{\rho_\infty}} \approx 300.243\ (\mathrm{Km/s})$
M_∞	Mach number of free stream condition	0.8
α	Angle of attack	$1.25\ (\mathrm{degree})$

In the field of computational fluid dynamics (CFD), large eddy simulation (LES) is an attractive tool to predict turbulent flow more realistically. Recently, applications of the LES to complicated geometries, such as an entire aircraft configuration, have become the focus of much research in the field of engineering. Indeed, unstructured meshes are widely used to manage complicated geometries.

The Euler equations, similarly, as other nonlinear hyperbolic systems of conservation laws, may have discontinuous solutions. As for the finite element method (FEM), the standard conforming finite element techniques were suitable for the numerical solution of elliptic and parabolic problems, linear elasticity and incompressible viscous flow, when the exact solution is sufficiently regular. Of course, there are also conforming finite element techniques applied to the solution of compressible flow. Stabilized finite element methods, such as the streamline upwind/Petrov‑Galerkin (SUPG) method [1] of the Galerkin /least-squares (GLS) method [2] are well established and already employed in certain industrial and commercial codes. However,

stabilized finite element methods have, traditionally, been employed with linear elements [3]. A comparison of low and higher order stabilized finite elements for the incompressible Navier‑Stokes equations is presented in [4], where it is shown that cubic elements are between six and seven times more efficient than linear elements. In a variety of the above test cases, higher order approximations bring, in the viewpoint of efficiency, for obtaining a given accuracy. But the treatment of discontinuous solutions is rather complicated discussed in [5].

Finite volume method (FVM) is popular because conservation laws are rigorously satisfied for the numerical solution of compressible flow. For a detailed treatment of finite volume techniques, we can refer to [6,7,8]. Moreover, the FVM is applicable on general polygonal meshes and its algorithms are easy. Therefore, many fluid dynamics codes and program package are based on the FVM. However, the standard FVM is only of the first order, which is not sufficient in a number of applications. The increase of accuracy in finite volume schemes applied on unstructured and /or anisotropic meshes seems to be problematic and is not theoretically sufficiently justified, and more cases a fundamental problem for the LES because high mesh density is required to resolve the large-scale motion containing most of the turbulent energy. This problem makes the FVM unfordable for LES with unstructured meshes.

A combination of idea and techniques of the FEM and the FVM yields the discontinuous Galerkin method (DGM) using advantages of both approaches and allowing to obtain schemes with a high‑order accuracy in a natural way. The DGM [8,9] is a high order unstructured mesh method. With the DGM, basis functions and degree of freedom (DOF) are introduced independently in each cell, and variables are reconstructed as the sum of the basis function multiplied by the corresponding
DOFs. This means that high-order reconstructions are possible without referring to variables in nearby cells, a feature that is often called compactness. The DGM has been widely applied to steady and unsteady flow problems with Reynolds averaged Navier‑Stokes simulations (RANS) studied in [10].

On the other hand, a non-dissipative or low dissipative numerical scheme is crucial to perform high fidelity simulations of turbulence in direct numerical simulation and LES. However, it is well known that standard central difference approximations induce numerical instability, additional numerical dissipation is required to stabilize flow simulations. Alternatively, numerical stability can be enhanced at least for smooth solutions by satisfying conservation of quadratic quantity such as the kinetic energy in a discrete sense. In the Euler equations, the total kinetic energy is preserved in the incompressible limit in a periodic domain. However, kinetic energy preservation is not always guaranteed in numerical simulations. Some kinetic energy preserving (KEP) schemes have been proposed for compressible flows and showed improvements in computational stability in [11-14]. Those KEP schemes are formulated based on central difference approximation and thus are non-dissipative. Although a standard central difference discretization is not numerically stable, the KEP schemes archives stable and non‑dissipative numerical simulations by preserving the kinetic energy in a discrete sense. Recently, a kinetic energy and entropy preserving (KEEP) scheme is proposed by [15]. To preserve both the kinetic energy and entropy, the KEEP scheme is designed such that the energy exchange between the kinetic energy and internal energy is properly calculated in the total energy equation. In [15], the KEEP scheme showed a further enhancement of numerical stability, compared to existing KEP scheme.

During last decade, there has been a great interest in developing efficient high order methods for computational fluid dynamics as mentioned above. However, the authors adopt a modified mathematical model for the compressible Euler equations together standard finite element strategy studied in [16]. For numerical experiments, we focus on a subsonic flow and a supersonic flow around an elliptic body in this paper. To implement a finite element-like program for the compressible Euler equations, [16] derives the following equations for the continuity equation, the momentum equation and an equation for the pressure:

$$\frac{Da_\rho}{Dt} + \nabla \cdot \boldsymbol{u} = 0, \tag{6}$$

$$\frac{1}{RT}\frac{D\boldsymbol{u}}{Dt} + \nabla a_p = 0, \tag{7}$$

$$\frac{Da_p}{Dt} + \gamma \nabla \cdot \boldsymbol{u} = 0, \tag{8}$$

using the new variables $a_\rho = \log(\rho)$ and $a_p = \log(p)$, where $RT = p/\rho$. Eq. (6) is interesting, because it is linear with respect to the variables a_ρ and $\boldsymbol{u}$. It appears again interesting to introduce the new variable a_p to get the linear equation (8). As a result, we obtain the original system (1-4) in the equivalent form (6-8). It is noteworthy that the equivalent form (6-8) are standard convection equations added external forces $\nabla \cdot \boldsymbol{u}$, ∇a_p, $\gamma \nabla \cdot \boldsymbol{u}$, respectively. Therefore, we need to consider physically compressible fluid, but can choice numerically an arbitrary numerical calculation scheme as incompressible flow. For temporal discretization for the material derivative $\frac{D}{Dt}$, the finite element characteristic curve method [17-19] is utilized to treat $\frac{D}{Dt}$ as a linear term. To complete the spatial discretization, we use the finite element formulation with the bubble function. It has recently been found the relationship [20-22] between the stabilized finite element method and the bubble function element [23] in the finite element method in [24]. In the steady advection diffusion problem, the bubble function element is equivalent to the streamline-upwind/Petrov-Galerkin (SUPG) finite element method with the P1 element. Some researchers have developed advanced bubble function elements for incompressible fluid flow [25-28]. The advanced bubble function elements are established using the bubble function with a scaling parameter according to the cell Peclet number to attain optimal numerical diffusion. From finite element theory, meshes with equilateral triangles are well known to be more suitable for isotropic problems. However, the notion of equilaterality involves lengths through scalar products in each metric. Therefore, anisotropic meshes might be regarded as isotropic with respect to a different metric. We can adapt the mesh to follow the solution if the metric is defined using aposteriori error estimation. An unstructured grid environment is the natural framework for the introduction of general adaptivity and the anisotropy concept. [29,39] described numerical procedures related to AMR with the metric. [32] presented its mathematical proof in continuous and discrete spaces of the domain. [29,31,33] used it for flow-field shape optimization. The present study also applies it to the compressible Euler system (6-8).

2 THE SUBSONIC FLOW PROBLEM AROUND NACA0012

Let $\Omega \subset \mathbb{R}^d (d = 2)$ be bounded domain and $\Gamma = \partial\Omega$ be the boundary of Ω, where Ω is expressed as:

$$\Omega = \Omega_{\mathrm{Rect}} \setminus \Omega_{\mathrm{wing}}, \tag{9}$$

$$\Omega_{\mathrm{Rect}} = \{\boldsymbol{x} = [x, y]^{\mathrm{T}} \subset \mathbb{R}^d; -400 \leq x < 400, -300 \leq y \leq 300\}, \tag{10}$$

$$\Omega_{\mathrm{wing}} = \{\boldsymbol{x} = [x, y]^{\mathrm{T}} \subset \mathbb{R}^d; 0 < x < 1, y_- \leq y \leq y_+\}, \tag{11}$$

$$y_\pm = \pm 0.6(0.2969 - 0.1260x + 0.3516x^2 + 0.2843x^3 - 0.1015x^4), \tag{12}$$

Let T be a positive constant. We consider the subsonic flow problem around NACA0012; find $(a_\rho, \boldsymbol{u}, a_p)$: $\Omega \times (0, T) \to \mathbb{R} \times \mathbb{R}^d \times \mathbb{R}$ such that

$$\frac{Da_\rho}{Dt} + \nabla \cdot \boldsymbol{u} = 0 \text{ in } \Omega \times (0, T), \tag{13}$$

$$\frac{1}{RT}\frac{D\boldsymbol{u}}{Dt} + \nabla a_p = 0 \text{ in } \Omega \times (0, T), \tag{14}$$

$$\frac{Da_p}{Dt} + \gamma \nabla \cdot \boldsymbol{u} = 0 \text{ in } \Omega \times (0, T), \tag{15}$$

$$\boldsymbol{u} \cdot \boldsymbol{n} = 0 \text{ on } \partial\Omega_{\mathrm{wing}} \times (0, T), \tag{16}$$

$$\boldsymbol{u} = M_\infty U_\infty \big[U_x(\alpha), U_y(\alpha)\big] \text{ on } \partial\Omega_{\mathrm{Rect}} \times (0, T), \tag{17}$$

$$\rho = \rho_0, \boldsymbol{u} = \boldsymbol{u}_0, p = p_0 \text{ in } \Omega \text{ at } t = 0, \tag{18}$$

where

$$U_x(\alpha) = \cos\left(\frac{2\pi}{360}\alpha\right), U_y(\alpha) = \sin\left(\frac{2\pi}{360}\alpha\right), \tag{19}$$

and α represents an angle of attack (AOA).

3 NUMERICAL SCHEMES

For all numerical calculations, FreeFEM++ [34] is used. A material derivative is approximated numerically by using the characteristic curve finite element scheme with the first order demonstrated in [17] and analysed mathematically about an error estimation in [18]. The scheme is useful for large scale computation, because at least P1 element can be employed and the matrix of resulting linear system is symmetric, of course P2b element is possible for discretization in space. This paper introduces finite element method with bubble function element stabilization method [24], where P1b and P2b denote P1 and P2 with the bubble function. For comparisons with finite element meshes, the authors select P1-P1b-P1 and P2-P2b-P2 for a density-a velocity-a pressure. And more, the authors are adopting adaptive mesh refinement (AMR) and the quadrature formula distributed in FreeFEM++ [34] for resolving

shock wave with high accuracy. After discretising in time and space, UMFPACK solver [35] is used

4 NUMERICAL RESULTS

In this section. the author performs a numerical calculation for a subsonic flow around NACA0012 in the compressible Euler field, and the three kinds of aerodynamics coefficients C_p, C_d, C_l are compared with previous numerical studies [36].

4.1 Finite element mesh

Fig. 1 shows (a) wide and (b) zoom finite element meshes with the number of vertex (NBVX) 151698. For resolving shock wave in high accuracy, finite element mesh around an inner boundary $\partial\Omega_{\mathrm{Wing}}$ of Ω is much finer than an outer boundary $\partial\Omega_{\mathrm{Rect}}$ of Ω. This paper generates 2 kinds of finite element meshes for NBVX = 151698 and 223090 listed in Table 2, where a time increment Δt is set to satisfy CFL condition, respectively.

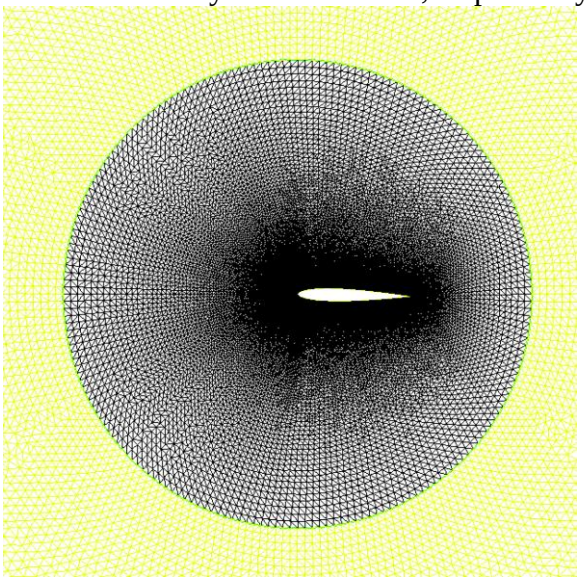

Figure 1: Zoom view of finite element mesh of NBVX = 151698.

4.2 Adaptive mesh refinement with times steps

Hereafter, a finite element mesh at the time step n is denoted by Ω_h^n for the sake of simplicity. In this paper, adaptive mesh refinement (AMR) is performed at each time steps for resolving shock wave with high accuracy. At first, the authors adaptive a finite element mesh Ω_h^{n-1} by using velocity $\boldsymbol{u}^{n-1}$ to obtain Ω_h^n which needs to calculate the compressible Euler field at the time step n. However, because of a slip condition defined on NACA0012, fine mesh enough to resolve a physical state of the compressible Euler flow is not generated. Thus, a shape of NACA0012 is degenerated with increasing time steps. Avoiding this numerical problem mentioned above, the authors performed adaptive mesh refinement to obtain the n-th finite element mesh Ω_h^n by using a previous time step velocity $\boldsymbol{u}^{n-1}$ and an initial finite element mesh

Ω_h^1 shown in Fig. 1. Ω_h^1 contains fine mesh around NACA0012, and by including it every time steps, it is possible to catch a time-dependent behaviour of density, velocity and pressure in shock wave. Fig. 2 shows adaptive meshes from $n = 10^3$ to 10^5 for P2-P2b-P2 for density-velocity-pressure. In figs. 2(a)-(c), two shock waves are moving from a nose-end and a trailing edge to ahead. From figs. 2(d)-(l), a shock wave created from a trailing edge is found on the upper and lower ends of NACA0012.

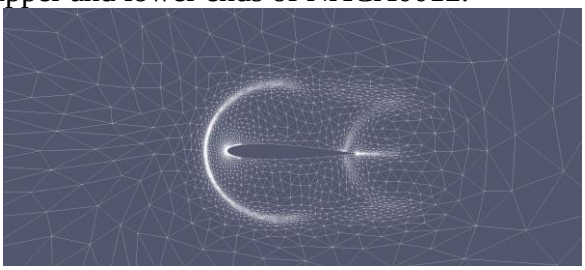

(a) $n = 1.0 \times 10^3$.

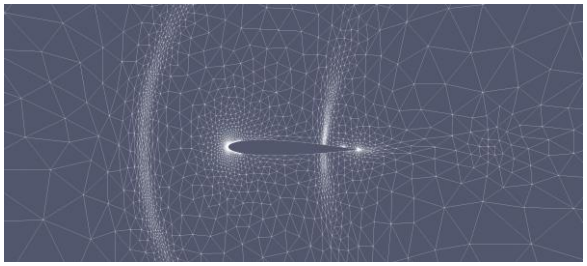

(b) $n = 5.0 \times 10^3$.

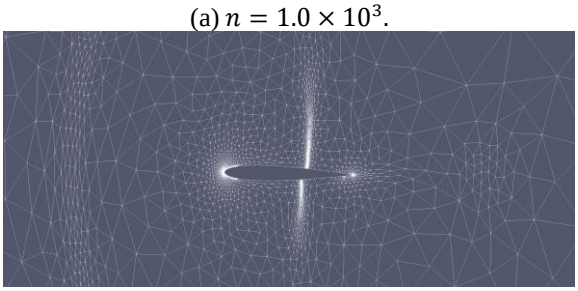

(c) $n = 10.0 \times 10^3$.

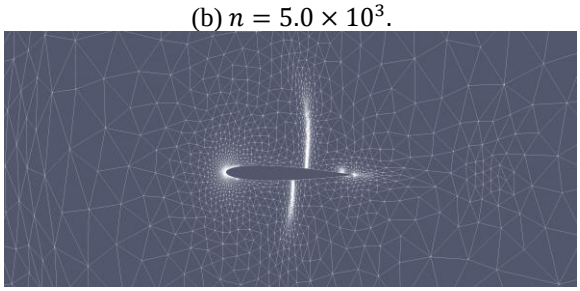

(d) $n = 15.0 \times 10^3$.

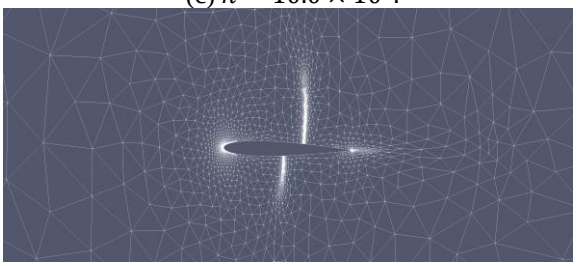

(e) $n = 20.0 \times 10^3$.

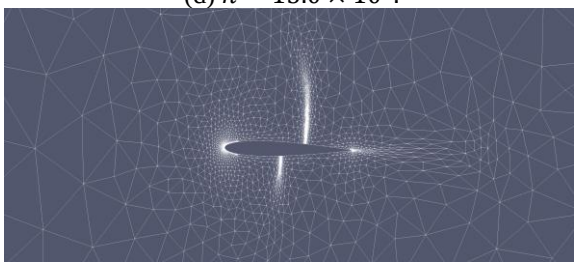

(f) $n = 25.0 \times 10^3$.

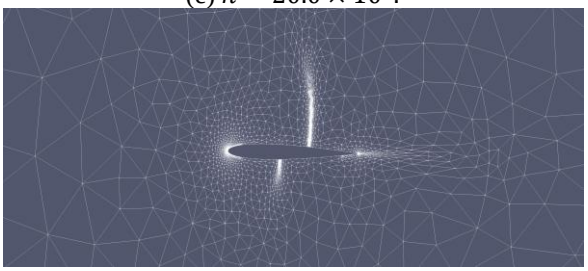

(g) $n = 30.0 \times 10^3$.

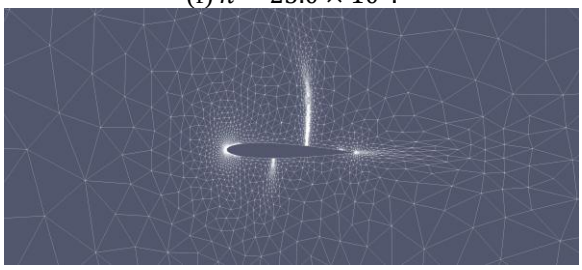

(h) $n = 35.0 \times 10^3$.

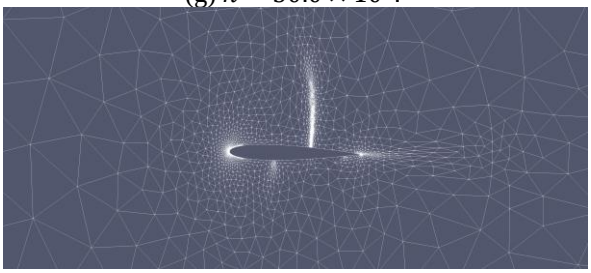

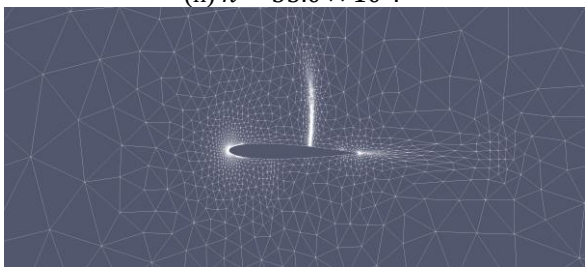

(i) $n = 40.0 \times 10^3$.

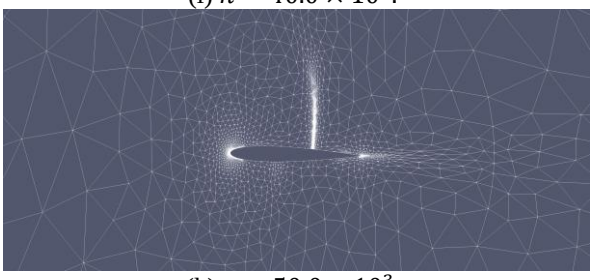

(j) $n = 45.0 \times 10^3$.

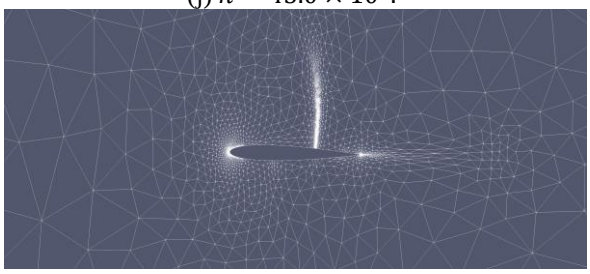

(k) $n = 50.0 \times 10^3$.

(l) $n = 100.0 \times 10^3$.

Figure 2: Adaptive meshes from $n = 1 \times 10^3$ to 100×10^3.

4.3 The compressible Euler field depending on finite element

Fig. 3 shows Mach number and finite element meshes at $n = 10^5$ for (a) P1-P1b-P1 and (b) P2-P2b-P2 for density-velocity-pressure. In the case of Fig. 3(a), shock waves on the upper and lower-ends are not created. On the other hand, fig. 3(b) shows an adequate shock wave around NACA0012. Fig. 4 compares pressure around NACA0012.

Table 2 lists representative aerodynamic coefficients like C_l and C_d. [36] compares C_l and C_d obtained numerically by building cube method with TAS solver [37]. As a result, relative errors C_l and C_d with Nakahashi et al. 2003 are about 6% and 9%. However, our numerical results are 1.197% and 0.15376%, which are much better than the previous study [36]. Fig. 5 compares pressure on NACA0012 for NBVX = 151698 and 223090, and both numerical results about pressure is similar to each other, even though pressure values are different slightly on the lower end.

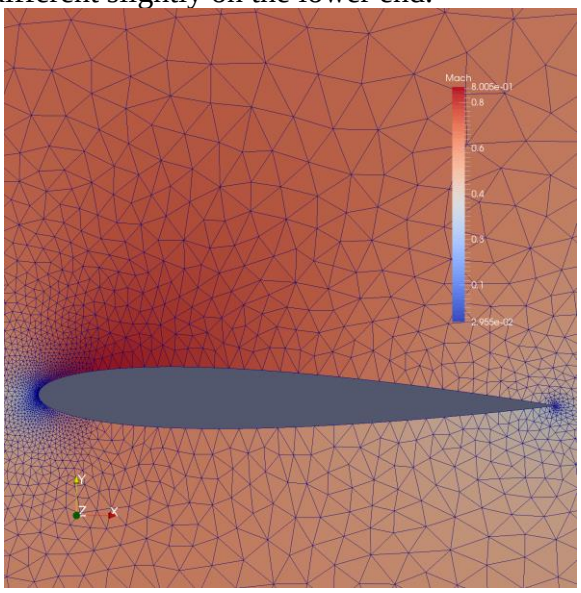

(a) P1-P1b-P1

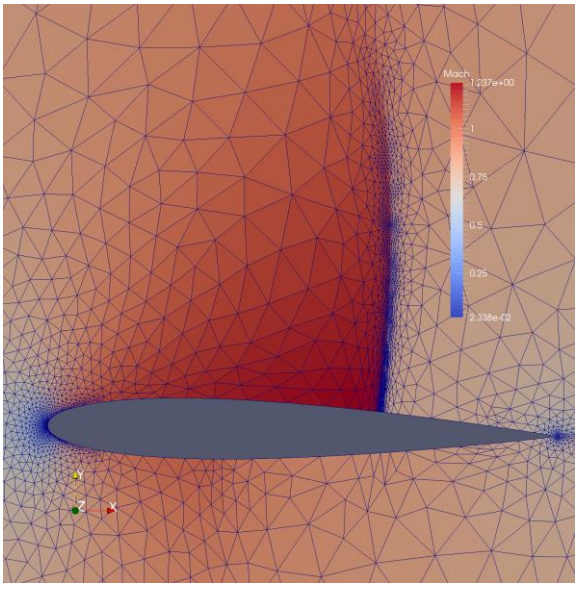

(b) P2-P2b-P2

Figure 3: Mach number and finite element meshes at $n = 100 \times 10^3$ for (a) P1-P1b-P1 and (b) P2-P2b-P2 for density-velocity-pressure.

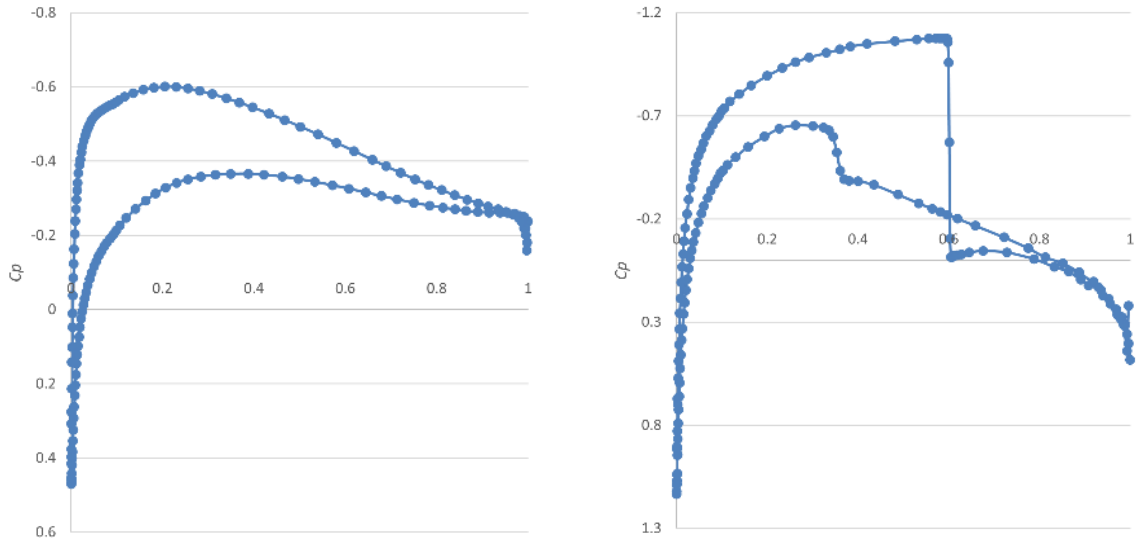

(a) P1-P1b-P1 (b) P2-P2b-P2

Figure 4: Pressure on NACA0012 at $n = 10^5$

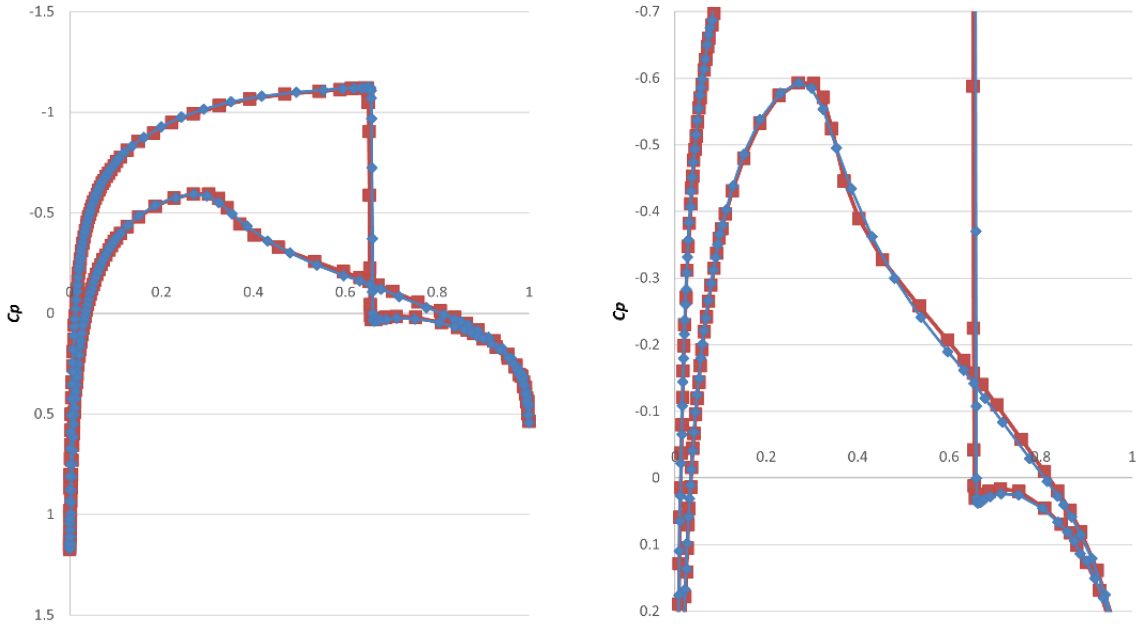

(a) wide view. (b) zoom view.

Figure 5: Comparison of pressure on NACA0012 at $n = 10^5$ for NBVX = 151698 and 223090.

Table 2: Variables and parameters.

Symbol	C_l	C_d
TAS	0.3621	0.0223
BCM(FINE)	0.3292(6.324%)	0.0202(9.417%)
This study	0.3501(1.197%)	0.0238(0.153%)

6 CONCLUSIONS

Numerical results of the compressible Euler system (6)‐(8) suggested by [16] were described in this paper, where the bubble function element stabilization method together with adaptive mesh refinement was introduced for increasing numerical stability and numerical accuracy. For a test case, NACA0012 was selected as a domain of interest, and numerical results using finite elements of P1‐P1b‐P1 and P2‐P2b‐P2 for density‐velocity‐pressure were compared at AOA=1.25 and Mach number 0.8. As a result, the shock wave is not found on the upper‐end and the lower‐end of NACA0012 in the former, and on the other hand the latter is adequate numerical result and relative error of C_l and C_d with previous study (Nishimura et al. (2011)) are 1.197% and 0.15376%. The mathematical model suggested by Vuyst (2013) is much simpler than the compressible Euler equation, because they are advection equations for a density, a velocity, and a pressure with each external forces. Therefore, the material derivative is considered for time stepping, and the characteristic curve method can be used. for decreasing calculation cost. It is expected to use this mathematical model together with the bubble function element stabilization method in many kinds of engineering and industry where the compressible Euler equation.

REFERENCES

[1] A. N. Brroks., T. J. R. Hughes, 1982. Streamline upwind/Petrov Galerkin formultions for convection dominated flows with particular emphasis on the incompressible NAvier-Stokes equations. Comput. Methods Appl. Mesh. Eng. 32:199‐259.

[2] T. Hughes, L. Franca, G. Hulbert, 1988. A new finite element formulation for computational fluid dynamics: VIII. The Galerkin/least-squares method for advection‐deffusive equations. Comput. Methods Appl. Mesh. Eng. 73:173‐189.

[3] T. Hughes, G. Scovazzi, T. E. Tezduyar. 2010. Stabilizedmethods for compressible flows. J. Sci. Comput. 40:343‐368.

[4] C. H. Whiting, K. E. Jansen. 2001. A stabilized finite element method for the incompressible Navier‐Stokes equations using a hierachical basis. Int. J. Num. Mehods. Fluids. 35:93‐116.

[5] M. Feistauer, J. Felcman, I. Straˇs. 2003. Mathematical and Computational Mathods for Compressible flow. Clarendon Press. Oxford.

[6] R. Eymard, T. Gallou´ ’ et, R. Herbin. 2000. Finite volume methods Handbook of Numerical Analysis. 713-1020, North-Holland, Amsterdam.

[7] M. Feistauer, J. Felcman. 1993. Mathematical Mathods in fluid dyanamics. Longman Scientific and Technical. Harlow.

[8] P. Lesaint, P. A. Raviart. 1974. On a finite element method fo solving the Nutron Transport equation. Mathematical aspects of finite elements in partial differential equations. Academic Press, New York. 89‐123.

[9] B. Cockburn, C. W. Shu. 1994. TVB Runge‐Kutta local projection discontinuous Galerkin finite element method for conservation laws. 2 General frame work. Math. Comp. 52:411‐435.

[10] H. Asada, S. Kawai. 2019. A simple cellwise high-order implicit discontinuous Galerkin

scheme for unsteady turbulent flows. Trans. Jpn. Soc. Aero. Space Sci. 62:93‐107.
[11] A. E. Honein, P. Moin. 2004. Higher entropy conservation and numerical stability of compressible turbulence simulations. J. Comp. Phy. 201:531‐208.
[12] A. Jainson. 2008. Formulation of kinetic energy preserving conservative scheme for gas dynamics and direct numerical simulation of one dimensional viscous compressible flow in a shock tube using entropy and kinetic energy preserving scheme. J. Sci. Comp. 34:188‐208.
[13] J. C. Kok. 2009. A high order low dissipation symmetry-preserving finite volume method for compressible flow on curvilier grids. J. Comp. Phy. 228:6811‐6832.
[14] Y. Abe, I. Morinaka,T. Haga,T. Nonomurad, Hi. Shibatad, K. Miyaji. 2018. Stable, non-dissipative, and conservative flux-reconstruction schemes in split forms Author links open overlay panel. J. Comp. Phy. 353:193‐227.
[15] Y. Kuya, K. Totani, S. Kawai. 2018. Kinetic energy and entropy preseving schemes for compressible flow by split convective forms. J. Comp. Phy. 375:823‐853.
[16] F. D. Vuyst. 2013: Numerical modeling of transport problems using freefem++ software ‐ with examples in biology, CFD, traffic flow and energy transfer. Master. Mod ´ elisation num ´ erique des probl ´ emes de transport sur freefem++. ENS CACHAN. 62. cel-00842234.
[17] H. Notsu. 2008. Numericla computations of cavity flow problems by a pressure stabilized characteristic-curve finite element scheme. Trans. JSCES. 20080032.
[18] H. Notsu, M. Tabata. 2015. Error estimates of a pressure-stabilized characteristics finite element scheme for Oseen equations. J. Sci. Comput. 65:940‐955.
[19] H. Notsu, M. Tabata. 2014. Error Estimates of a Stabilized Lagrange‐Galerkin Scheme of Second-Order in Time for the Navier‐Stokes Equations. Math. Fluid Dyn. Present and Future. 497-530.
[20] R. Pierre. 1988. Simple C0 approximations for the computation of incompressble flows. Comput. Methods Appl. Mech. Engrg. 68:205-227.
[21] F. Brezzi, M. O. Bristeau, L. P. Franca, M. Mallet, G. A. Roge. 1992. A relationship between stabilized finite element methods and the Galerkin method with bubble functions, Comput. Methods Appl. Mech. Engrg. 96:117-129.
[22] C. Baicocchi, F. Brezzi, L. P. Franca. 1993. Virtual bubbles and Galerkin-Least-Squares type method(Ga.L.S.). Comput. Methods Appl. Mech. Engrg. 105:125-141.
[23] D. N. Arnold, F. Brezzi, M. Fortin. 1984. A Stable Finite Element for the Stokes Equations, Cal-colo. 23:337‐34.
[24] J. Matsumoto. 2005. A relationship between stabilized FEM and Bubble function element stabilization method with orthogonal basis for incompressible flows. J.Appl. Mecha. 8:233‐242.
[25] J. C. Simo, F. Armero, C. A. Taylor. 1995. Stable and time-dissipative finite element methods for the incompressible Navier-Stokes equations in advection dominated flows, Int. J. Numer. Meth. Engng., 38:1475‐1506.
[26] T. Yamada. 1998. A bubble element for the compressible Euler equations. Int. J. Comput. Fluid Dyn. 9:273‐283.
[27] F. Brezzi, L. P. Franca, L.P, A. Russo. 1998. Further considerations on residual-free

bubbles for advective diffusive equations. Comput. Methods Appl. Mech. Engrg. 166:25-33.

[28] H. Okumura, M. Kawahara. 2003. A new stable bubble element for incompressible fluid flow based on a mixed Petrov-Galerkin finite element formulation. Int. J. Comput. Fluid Dyn. 17:275-282.

[29] M. J. Castro-Diaz, F. Hecht, B. Mohammadi, O. Pironneau. 1997. Anisotropic Unstructured Mesh Adaptation for Flow Simulations. Int. J. Numer. Meth. Fluids. 25: 475-491.

[30] M. J. Castro-Diaz, F. Hecht. 2006. Anisotropic Surface Mesh Generation. INRIA Res. Rep. 2672:1-31.

[31] J. P. Frey, F. Alauzet. 2003. Anisotropic mesh adaptation for transient flows simulations. In Proc. of 12th Int. Meshing Roundtable. 12:335-348.

[32] F. Alauzet, A. Loseille, A. Dervieux, J. P. Frey, J. P. 2006. Multi-Dimensional Continuous Metric for Mesh Adaptation. In Proc. of 15th Int. Meshing Roundtable. 15:191-214.

[33] B. Mohammadi, F. Hecht. 2001. Mesh Adaptation for Time Dependent Simulation, Optimization and Control. Revue Europeenne deselements finis. 10:575-595.

[34] F. Hecht. 2012. New development in FreeFem++. J. of Numerical Math. 20:251-265.

[35] T. Davis. 2004. Algorithm 832: UMFPACK, an unsymmetric-pattern multifrontal method. ACM Trans. On Math. Software. 30:196-199.

[36] Y. Nishimura, D. Sasaki, K. Nakahashi. 2011. Euler calculaton using the compressible Building Cube Method around the airfoil and wing. JAXA-SP-11-015.

[37] K. Nakahashi, et al. 2003. Some challenge of realistic flow simulations by unstructured grid CFD. In. J. for Num. Method. in Fluids. 43:769-783.